Geothermal Energy

RESEARCH

Open Access

Experimental study on convective heat transfer of an open-loop borehole heat exchanger

Xianbiao Bu[1,2*], Kunqing Jiang[1,2], Huashan Li[1,2*], Feng Ma[3] and Lingbao Wang[1,2]

*Correspondence:
buxb@ms.giec.ac.cn;
lihs@ms.giec.ac.cn

[1] School of Energy Science and Engineering, University of Science and Technology of China, Guangzhou 510640, China
[2] Guangzhou Institute of Energy Conversion, Chinese Academy of Sciences, Guangzhou 510640, China
[3] Institute of Hydrogeology and Environmental Geology, Chinese Academy of Geological Sciences, Shijiazhuang 050061, China

Abstract

Open-loop borehole heat exchanger (OBHE) is a single well geothermal heat exchanger with an open-loop structure that can realize the geothermal energy extraction without mining the geothermal water. In this paper, a sandbox experiment is designed to simulate the convective heat transfer process in the reservoir area of OBHE. The mechanism of convective heat transfer in the reservoir area is studied, and the key factors that affect the convection heat transfer intensity are analyzed. The results show that the convection heat transfer of OBHE in the reservoir area is affected by both the driving effect of fluid flow inside the screen tube and the buoyancy effect. In the forward flow mode, the two effects have the opposite direction. While in the backward mode, the two effects have the same direction. The backward flow mode is more conducive to convective heat transfer. In addition, many factors influencing significantly the convective heat transfer of OBHE include inlet temperature, inlet flow rate, reservoir temperature, fluid flow direction and inner tube diameter.

Keywords: Deep borehole heat exchanger, Open-loop borehole heat exchanger, Sandbox experiment, Convection heat transfer

Introduction

The recent Glasgow Climate Pact reaffirms the long-term global goal to hold the increase in the global average temperature to well below 2 °C above pre-industrial levels and to pursue efforts to limit the temperature increase to 1.5 °C above pre-industrial levels. To achieve the above goals, it is necessary to reduce the use of fossil energy and increase the proportion of renewable energy in the energy supply. However, the current use of fossil fuels such as oil, coal, and natural gas accounts for 80% of global energy consumption (Suganthi and Samuel 2012). As one of the renewable energy sources, geothermal energy reserves are huge and widely distributed. It can be used for power generation, space heating and industrial processes, etc. (Barbier 2002). When combined with ground source heat pumps, geothermal energy can be used anywhere, while geothermal power generation is only applicable to high-temperature geothermal resources. And many countries around the world have recognized its enormous potential for future

energy supply, energy conservation, and emission reduction (Barbier 2002; Stefánsson 2005; Xia and Zhang 2019).

Geothermal resources can be divided into shallow, hydrothermal and hot dry rock geothermal resources (Wang et al. 2020). The shallow geothermal energy utilization approach has drawbacks such as imbalanced building cooling and heating loads and large land occupation, limiting its use in areas with high heating demand and urban areas with limited land resources (Liu et al. 2015; Deng et al. 2020; Ma et al. 2020), and the exploitation of hydrothermal geothermal resources also faces problems such as difficulty in recharging (Huang et al. 2021). Thus, it is necessary to develop a new method to explore geothermal energy in order to avoid the above problems. Deep borehole heat exchanger (DBHE) uses circulating fluid in a closed coaxial casing to extract heat from the ground. No water is extracted from the reservoir during the heat extraction process, and the problem of recharge is thus avoided (Bu et al. 2012). Besides, DBHE needs less construction area than the shallow geothermal utilization system, so it is suitable for urban areas with high population density (Morchio and Fossa 2019; Morchio et al. 2022; Lund et al. 2020).

The length of DBHE can be 3000 m or even longer. Because the geothermal gradient is positive and nearly constant in the subsoil, the undisturbed ground temperature typically almost rises linearly with depth (Morchio et al. 2022). The ground temperature rises by about 3 °C for every 100 m increase in the ground depth (Luo et al. 2020). So the temperature of the rock at the bottom of a geothermal well with a depth of 3000 m can reach about 100 °C. By circulating fluid inside the DBHE, sufficient heat can be extracted from the high-temperature rocks around the single well, and the heat extracted by DBHE from underground can be used for building heating or geothermal power generation, etc. (Cheng et al. 2013; Bu et al. 2019). So far, numerous studies on the heat transfer performance of DBHE have been reported, including experiments (Morita et al. 1992a, b), numerical simulation (Kujawa et al. 2006; Davis and Michaelides 2009; Noorollahi et al. 2015; Nian and Cheng 2018; Hu et al. 2020), analytical solution (Luo et al. 2019, 2020; Pan et al. 2019), and combined methods (Wang et al. 2017; Cai et al. 2019; Huang et al. 2020), and their findings have proven the feasibility of DBHE. In Hawaii, Morita et al. (1992a, b) conducted experiments on DBHE with a depth of 876.5 m. Due to the excellent geothermal conditions, the bottom hole temperature of the single well could reach 110 °C. The study by Kujawa et al. (2006) showed that for a 3950-m-long geothermal well, the outlet temperature of DBHE can reach 53.0 °C and the heat exchange rate is 644 kW under the conditions of inlet temperature of 25 °C and flow rate of 20 m^3/h. The performance of DBHE is relatively stable and after 10 years of continuous operation, the decrease in outlet temperature of DBHE can be less than 3% (Cai et al. 2019). Furthermore, it is reported that the energy efficiency of a ground source heat pump combined with DBHE is also superior to that of a traditional shallow ground source heat pump system (Wang et al. 2017).

Despite the fact that the above research indicates that DBHE has a relatively reliable heat transfer performance, its low power and high investment hindered its utilization (Dai et al. 2019a, b). In order to obtain sufficient heat exchange rate, it is necessary to drill deep geothermal wells when constructing DBHE. The high drilling and construction costs limit the promotion and application of DBHE (Kujawa et al. 2006). Although it is

possible to reduce construction costs by converting abandoned oil wells into DBHE (Bu et al. 2012), this method is not suitable for large-scale applications. Therefore, efforts are needed to improve the heat transfer performance of DBHE to reduce investment risks and promote its popularization. Some researchers have attempted to optimize the operating and structural parameters of DBHE in order to accomplish this goal (Fang et al. 2018; Liu et al. 2019; Kalmar et al. 2020; Liu et al. 2020; Pan et al. 2020). It is believed that improving the thermal insulation performance of the inner tube can reduce the heat loss of the DBHE, thereby increasing its heat exchange rate (Kalmar et al. 2020). And the flow mode that circulating fluid flows downward through the annulus between the two pipes was recommended (Fang et al. 2018). In addition, a sensitivity analysis conducted by Pan et al. (2020) showed that the diameter of the outer tube, flow rate and well depth also have a great impact on the heat extraction rate of DBHE.

The heat extraction process of DBHE mainly relies on the heat conduction of the rock, and the poor heat conduction ability of the rock results in the low heat transfer rate of a single well. Therefore, enhancing the ability to transfer heat on the rock side of the DBHE can effectively increase the heat transfer rate of a single well (Bu et al. 2019). And some researchers have proposed improvement schemes of DBHE based on this criterion, such as injecting composite high thermal conductivity materials into the seepage layer to improve the thermal conductivity of the surrounding rock (He and Bu 2020) and building artificial reservoir (Cheng et al. 2016; Huang et al. 2018). Moreover, Dai et al. (2019a, b) proposed an open-loop deep borehole heat exchanger (OBHE), which have a similar structure to DBHE except that it adapts an open structure in the reservoir area, and the open-loop structure was found to be conducive to the heat exchange of geothermal wells. OBHE is also similar to the standing column well (SCW), which is the underground heat exchanger part of groundwater heat pump systems that groundwater is drawn from and returned to the same well in a semi-open-loop arrangement (Deng et al. 2005). The pumping action, which facilitates the movement of groundwater into and out of the borehole and induces advective heat transfer, increases the heat exchange rate in the standing column well (Rees et al. 2004). According to the above research, the open structure is beneficial to the heat extraction of a single well and improving the heat transfer capacity of the rock side of DBHE can indeed increase the heat transfer rate of a single well.

Among the above improvement schemes of DBHE, the OBHE is the easiest to construct because it does not involve fracturing or other forms of transformation of the rock. Besides, OBHE can realize the exploitation of geothermal energy without mandatory compulsory extraction of groundwater from the reservoir, and water can freely flow into or out of geothermal wells, which is suitable for areas with difficult reinjection problems. OBHE may have some disadvantages caused by its open-loop structure, such as clogs, it is believed that these disadvantages can be solved by using the experience of dealing with these problems in other open-loop geothermal systems. So it is worth putting more attention to this kind of single well geothermal heat exchanger. OBHE can be regarded as composed of two parts: the reservoir area (open-loop structure) and the tight rock area (close-loop structure). The mechanism of heat transfer for OBHE in the tight rock area is the same as DBHE, which has been fully studied. However, at present, the mechanism of heat transfer for OBHE in the reservoir area remains unclear and

needs to be studied further. Therefore, this article focuses on the study of the OBHE heat transfer process in the reservoir area.

For the study of geothermal heat exchangers, the sandbox experiment allows for performing tests under more controlled conditions and adjusted more easily and economically than those achievable in full-scale experiments (Morchio et al. 2021). Morchio et al. (2021) developed a suitable scale model of a real borehole heat exchanger (BHE) and the surrounding ground for small-scale TRT experiments. Shirazi and Bernier (2014) designed a small-scale laboratory sandbox apparatus to study transient heat transfer inside and outside boreholes. Beier et al. (2011) constructed a large laboratory sandbox with a borehole of length 18 m and conducted detailed thermal response test experiments. This shows that sandbox experiment is an effective method in the study of geothermal heat exchangers.

Thus, a sandbox simulation experiment is carried out in this paper to simulate the convective heat transfer process of OBHE in the reservoir area. Different from the sandbox experiment conducted by the above researchers, which mainly focus on the heat conduction process of BHE, the sandbox experiment at present work focus on analyzing the convective heat transfer process of OBHE in the reservoir. Although some researchers have studied the geothermal heat exchanger with open-loop structure (Song et al. 2019) or considered the convective heat transfer around the geothermal heat exchanger (Zhao et al. 2008) by sandbox experiments, the structure of the heat exchangers they studied differs from that of the OBHE in the reservoir area, and the objective of their experiment is also clearly different from that of the current study.

The purpose of the experiment in this paper is to study the heat transfer mechanism of OBHE in the reservoir area, especially the interaction of flow and heat transfer between fluids inside and outside the well. And factors affecting OBHE heat transfer intensity in the reservoir area are also under consideration. For the above purposes, experimental conditions such as different flow rates, different circulation fluid flow directions and different inlet water temperatures are considered. Although there are some differences between laboratory model tests and actual geological conditions, the laws obtained from the experiments are of great practical significance. The results of the sandbox experiment can also provide references for the research of other open-loop geothermal heat exchangers with a similar open structure, such as SCW. The numerical simulation results on OBHE have been published in reference (Jiang and Bu 2022), and the results have proved that OBHE has better heat transfer performance. This paper mainly focuses on the combined influence of the driving effect of fluid flow inside the screen tube and the buoyancy effect on the fluid flow and heat transfer inside and outside the well by experimental research. To the best of the authors' knowledge, no previous researcher has focused on this issue.

OBHE concept

The structure of OBHE is shown in Fig. 1. OBHE has a coaxial structure formed by an inner and an outer tube, and the outer tube in the reservoir area is a screen tube with an open structure. Water as a working fluid can be injected from the annulus or inner pipe, and correspondingly extracted from the inner pipe or annulus. Water is continuously heated by the thermal energy from the underground as it flows through OBHE. In the

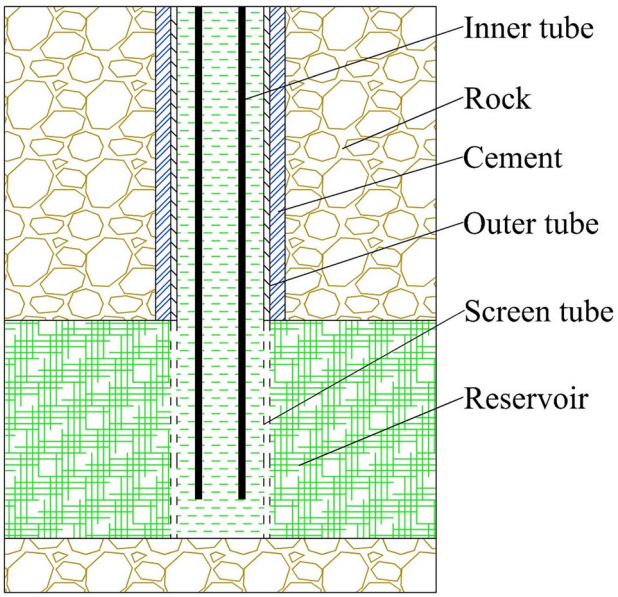

Fig. 1 Structure diagram of OBHE

non-reservoir area of OBHE, heat is transferred from rock to OBHE by heat conduction. And in the reservoir area, the open-loop structure of OBHE allows the geothermal fluid to freely flow back and forth between the reservoir and the well and thus achieve convection heat transfer in the reservoir near the single well, which has a positive effect on the heat extraction process (Dai et al. 2019a, b).

Experiment setup

As mentioned earlier, the purpose of the sandbox experiment is to study the heat transfer mechanism and the factors that affect the heat transfer intensity of OBHE in the reservoir area instead of accurately predicting the heat transfer rate of OBHE. Therefore, the sandbox experiment only simulates the convective heat transfer in the reservoir area of OBHE.

The sandbox experimental device is shown in Figs. 2 and 3. The main body of the experimental device includes a sandbox, hot water tank, chiller, water tank, and a measuring system composed of a flowmeter and thermal resistances. In order to study the influence of different fluid flow directions in the annulus on heat transfer, the cold water circulation pipeline is designed to be able to freely switch the fluid flow direction. The four connection points *a*, *b*, *c*, and *d* in the figure are flexible connections. The fluid flow direction can be reversed only by swapping the hoses connected to the *a* or *b* point. When the heat exchange fluid flows from top to bottom in the annulus, it is called forward flow, and vice versa, it is called backward flow.

The main body of the sandbox was made of stainless steel, with a diameter of 1.6 m and a height of 0.8 m. The sandbox was filled with glass beads with a diameter of 1–1.5 mm and hot water to simulate the reservoir. Volumetric method was used to determine the porosity of artificial glass micro-balls, and the porosity here means the ratio of the volume of pore space between the glass beads to the volume of the glass beads. The specific

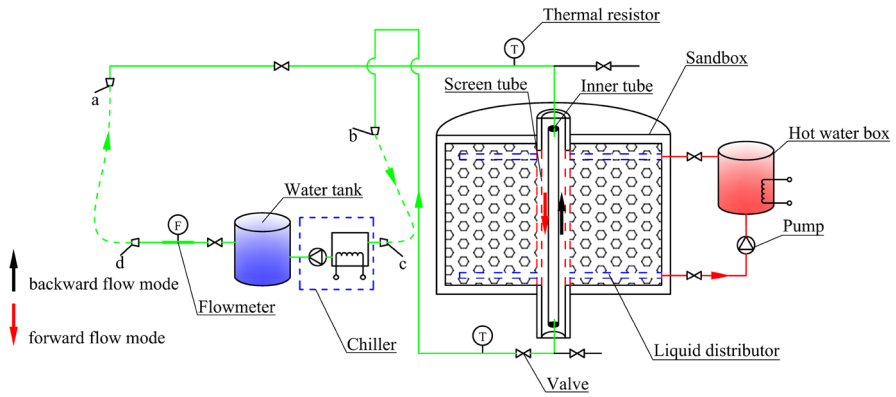

Fig. 2 System diagram of sandbox experimental device

Fig. 3 Photo of sandbox experiment system

method is to fill a graduated cylinder with glass beads, slowly inject water, weigh before and after water injection to determine the quality of the water, and then calculate the volume of the pore space. After several tests, the porosity of the glass beads was calculated to be 0.377 by averaging the results. A hot water circulating pump was used to extract the water in the hot water box to heat the sandbox, the rated flow of the hot water circulating pump was 3 m^3/h. At the same time, the water temperature of the hot water box was kept constant by the temperature control system. When the inside of the sandbox was heated to the specified temperature, turn off the hot water circulation pump and start the experiment at the same time. The duration of a single experiment was 1 h.

The outer tube of the coaxial casing adopted a screen tube with an open structure, allowing water to flow freely between the annulus and the sandbox while preventing the glass beads in the sandbox from entering the annulus. The inner diameter of the screen is 33.5 mm and the outer diameter is 38 mm. The chiller was used to control the inlet water temperature of the screen tube. And a water tank was arranged at the outlet of the chiller to eliminate the fluctuation of the outlet water temperature of the chiller. During the experiment, the cold water in the water chiller was pumped out by the cold water

circulating pump to flow first into the water tank and then enter the screen tube, after participating in the heat exchange processes inside the sandbox, it returned to the water chiller.

The main focus of this paper is the convective heat transfer between the fluid in the annulus of OBHE and the reservoir rather than its complete heat extraction process. Therefore, the coaxial tube was reasonably simplified by ignoring the flow process of the fluid in the inner tube and the heat transfer between fluid in the inner tube and annuls, leaving only the flow of the fluid in the annulus and heat and mass transfer inside and outside the screen to be studied. Based on this, the inner tube of the coaxial casing was replaced by a solid steel pipe, and an annular space structure was formed between the solid inner tube and the screen tube. Similar simplification methods have also been used by Song et al. in their sandbox experiments (Song et al. 2019). In addition, the inner tube was fixed in the form of a flexible connection, which facilitates the replacement of inner tubes with different sizes in the experiment. The outer diameters of the inner tubes involved in the experiment are, respectively, 17, 20 and 23 mm.

The measurement of flow and temperature was, respectively, completed by an electromagnetic flowmeter and thermal resistors. The electromagnetic flowmeter was arranged at the outlet of the water tank. A total of 40 thermal resistors were arranged in the entire experimental device. Two thermal resistors were arranged at the inlet and outlet of the screen tube to record the change in the inlet and outlet water temperature. The remaining thermal resistors were arranged inside the sandbox to record the change of temperature field inside the sandbox during the experiment. All thermal resistances in the experiment were connected to a paperless recorder. The accuracy of the temperature measurement was calibrated with a mercury thermometer. The standard deviation of the temperature measurement results is calculated as 0.062 °C. Considering the uncertainty brought by the thermal resistance itself, and the uncertainty caused by temperature calibration, the standard uncertainty of the estimated temperature measurement is ± 0.12 °C. And the uncertainty of the measured flow rate is estimated to be $\pm 1.5\%$.

The temperature measurement point layout inside the sandbox is shown in Fig. 4. For the convenience of description, the three straight lines formed by the longitudinally distributed temperature measuring points are marked as L1, L2, and L3, respectively. And the straight line formed by the horizontally distributed temperature measuring points is marked as temperature measuring line L4. Each spot in the figure represents a temperature measurement point. Among them, there are three temperature measurement points located at the intersection of the straight lines, which are the temperature measurement points shared by each line. The radial distances of lines L1, L2, and L3 from the outside diameter of the screen tube are 5, 10, and 15 cm, respectively, and the distance between line L4 and the bottom of the sandbox is 10 cm. The distance between two temperature measurement points on line L1 is 5 cm, and the distance between the lowest measurement point for L1 and the bottom of the sandbox is 5 cm. The distance between two temperature measurement points on lines L2 and L3 is 10 cm, and the distance between the lowest measurement point for L2 and L3 and the bottom of the sandbox is 10 cm. The distance between the first 8 temperature measurement points on line L4 from the left end is 5 cm, and the distance between the subsequent temperature measurement points is 10 cm.

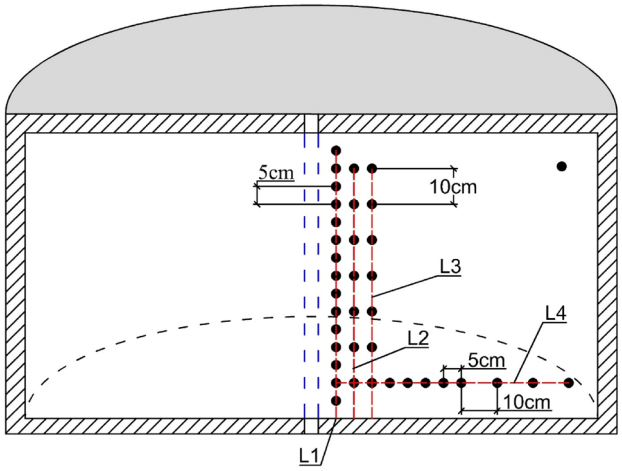

Fig. 4 Distribution of temperature measurement points inside the sandbox

Dimensionless parameters

In the following discussion, some dimensionless numbers will be partially used, and it may be useful to provide a complete list of dimensionless parameters in this section.

The temperature change of temperature measuring points inside the sandbox is expressed as the dimensionless temperature θ:

$$\theta = \frac{T_{\text{box}} - T_{\text{point}}}{T_{\text{box}} - T_{\text{in}}},$$

where T_{box} (°C) is the initial temperature of the sandbox, T_{in} (°C) is the inlet temperature of the fluid in the screen tube, T_{point} (°C) is the temperature at the temperature measuring point, that is, the temperature measured by the thermal resistors.

When discussing different outlet temperatures under the same inlet temperature and sandbox temperature, the following dimensionless outlet temperature is used:

$$\theta_{\text{o}} = \frac{T_{\text{out}} - T_{\text{in}}}{T_{\text{box}} - T_{\text{in}}},$$

where T_{out} (°C) is the outlet temperature of the screen tube.

Dimensionless height of temperature measuring point: $\delta = \frac{H_{\text{point}}}{H_{\text{box}}}$,

where H_{point} (mm) is the height of the temperature measuring point relative to the bottom of the sandbox, and H_{box} (mm) is the height of the sandbox.

The dimensionless radial distance between the temperature measuring point and screen tube axis: $\varphi = \frac{R_{\text{point}}}{R_{\text{box}}}$,

where R_{point} (mm) is the radial distance between the temperature measuring point and screen tube axis, R_{box} (mm) is the radius of the sandbox.

The heat exchange intensity can be expressed in Nu number: $\text{Nu} = \frac{hd_{\text{h}}}{k_{\text{f}}}$,

where d_h (mm) is the hydraulic diameter, k_f (W/(m °C)) is the thermal conductivity of water, h (W/(m^2 °C)) is the heat transfer coefficient and can be calculated by the following equation:

$$h = \frac{P}{A(T_{tank} - T_f)} = \frac{q_v \times \rho_f \times C_f \times (T_{out} - T_{in})}{A \times (T_{tank} - T_f)},$$

where A (m^2) is the internal surface area of the screen tube, T_f (°C) is the average value of the inlet and outlet temperatures of the screen tube. q_v (m^3/s) is the volume flow rate, ρ_f (kg/m^3) is the density of water, C_f (J/(kg °C)) is the specific heat capacity of water. The heat exchange rate of the device is also calculated using the above formula.

The fluid Reynold number in the screen tube: $\mathrm{Re} = \frac{\rho_f u d_h}{\mu}$,

where d_h (m) is the hydraulic diameter, u (m/s) is the velocity of the fluid in the screen tube.

The experiment time is expressed by Fourier number (Sutton et al. 2003):

$$\mathrm{Fo} = \frac{\alpha_{eff} t}{{r_{tube}}^2},$$

where α_{eff} (m^2/s) is the effective thermal diffusivity, t (s) is the experiment time, r_{tube} (m) is the inner radius of the screen tube. And α_{eff} is defined as the following formula:

$$\alpha_{eff} = \frac{[\phi k_f + (1-\phi) k_s]}{[\phi \rho_f c_f + (1-\phi) \rho_s c_s]},$$

where Φ is the porosity of the glass beads, k_f (W/(m °C)) is the thermal conductivity of water, k_s (W/(m °C)) is the thermal conductivity of glass beads, ρ_s (kg/m^3) is the density of glass beads, c_s (J/(kg °C)) is the specific heat capacity of glass beads. The calculated effective thermal diffusivity is 4.22×10^{-7} m^2/s.

Results and discussion

In this study, the influence of different fluid flow directions on the convective heat transfer inside and outside the screen tube is considered, so the experimental device has two operating modes. As defined before, when the heat exchange fluid flows from top to bottom in the annulus, it is called forward flow, and vice versa, it is called backward flow. The forward flow mode corresponds to the annulus of the OBHE being the injection well, while the backward flow mode corresponds to the inner tube being the injection well. According to the relevant research on DBHE, the forward flow mode is more conducive to its heat extraction performance (Holmberg et al. 2016; Kalmar et al. 2020). However, it may be different for OBHE, because the convection heat transfer process occurs in the reservoir area of OBHE. Therefore, the study of the influence of flow directions on the heat transfer process of the reservoir is necessary.

Before the start of the formal experiment, the inlet temperature and flow rate control effect of the experimental device is verified. Figure 5 shows the variation of inlet temperature and flow rate with time under the conditions of setting the inlet flow rate Q to 0.4 m^3/h and the inlet temperature T_{in} to 14 °C. It can be seen from the figure that the inlet temperature and inlet flow rate are very stable during the experiment within 1 h

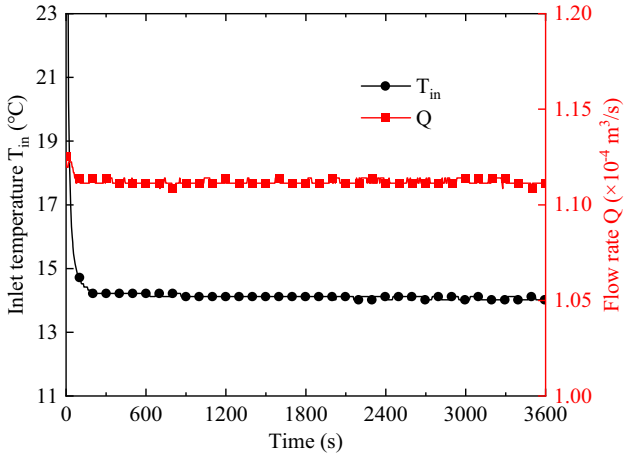

Fig. 5 Inlet temperature and inlet flow diagram

and the deviation between the measured value and the set value is extremely small. Only the test result at the initial stage has a large deviation, which is caused by the residual water in the pipeline at the beginning of the experiment. With the continuous operation of the experimental device, the measurement result returns to normal. This demonstrates that the inlet temperature and flow rate can keep stable during the process of experiment.

Analysis of convection heat transfer characteristics in the sandbox

After completing the verification and adjustment of the experimental system, experiments are carried out under different inlet flow conditions in the forward flow mode. The inlet flow rates are, respectively, 0.25, 0.35, 0.45 m^3/h, the outer diameter of the inner tube is 20 mm, and the corresponding Reynolds numbers are 1646, 2304, 2962, respectively. The sandbox temperature is 55 °C, and the temperature of inlet water for screen tube is 14 °C. Figure 6 shows the temperature variation of outlet water for screen tube with time. As can be seen in the figure, the initial outlet temperature is relatively high, and it decreases rapidly in a short period and then gradually becomes stable. As mentioned earlier, the relatively high initial outlet temperature is caused by the residual water in the pipeline. Therefore, this part of the data is removed when calculating the average outlet temperature and average power extracted from the experimental sandbox. The average temperature and average power are calculated from the 180 s after the start of the experiment. It can be also seen in the figure that the change in outlet water temperature is not linear with the change in Re. The outlet temperature is greatest when Re is 1646 and lowest when Re is 2304. However, some researchers point out that the outlet temperature of DBHE generally decreases with the increase of inlet flow (Bu et al. 2012; Cheng et al. 2013). This means that the heat exchange process of OBHE in the reservoir area is very different from the pure heat conduction process of DBHE, and thus further research is needed to more accurately reveal the mechanism of heat transfer for OBHE, especially in the reservoir area.

Figure 7 depicts the change of temperature at the temperature measurement point on L1 with time under different Re numbers. As can be seen in the figure, when Re

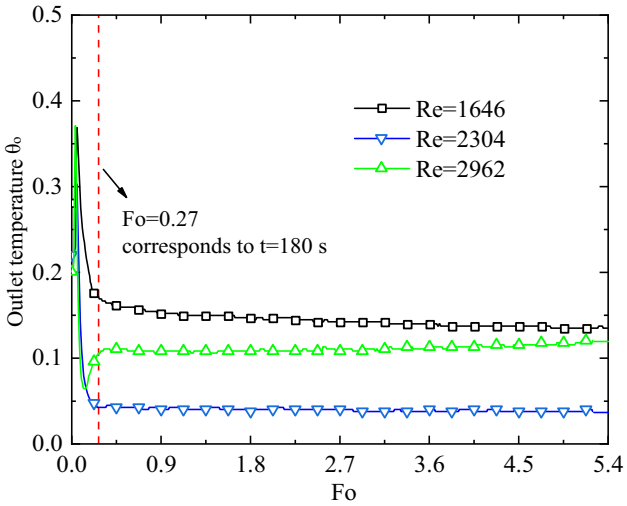

Fig. 6 Variation of outlet water temperature with time in forward flow mode

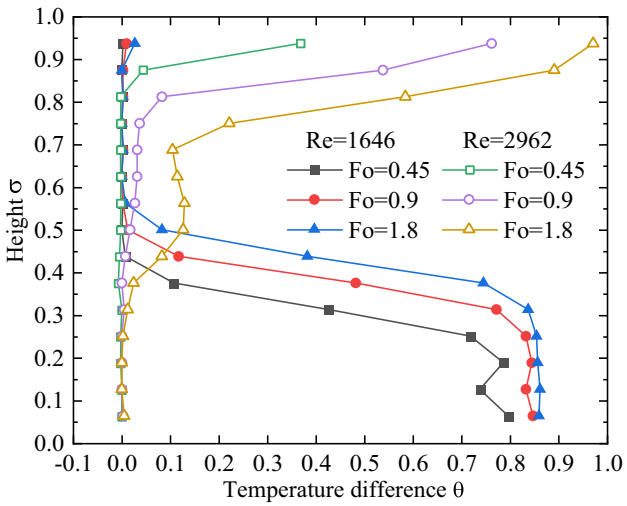

Fig. 7 Temperature change of L1 with time under different Re numbers in forward flow mode

is 1646, only the temperature measurement point near the bottom of the sandbox has a temperature change and this temperature change gradually increases with the increase of operating time, while the temperature of the temperature measurement point near the top of the sandbox hardly changes. The change of temperature difference θ shows that the thermal influence on the inside of the sandbox increases significantly with the increase of operation time. Moreover, the temperature change of L1 is the contrary while the Re increases to 2962. This shows that the difference in inlet flow rate in the forward flow mode has a great impact on the convective heat transfer inside and outside the screen tube. In order to further study the above phenomenon and explain such behavior, the experimental conditions with Re of 1975, 2633 and 3291 are supplemented, and other conditions remain unchanged. The results are shown in Fig. 8.

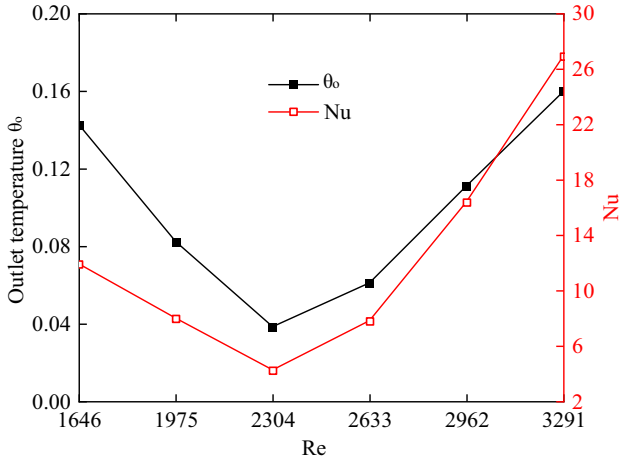

Fig. 8 Variation of average outlet water temperature and Nu with Re in forward flow mode

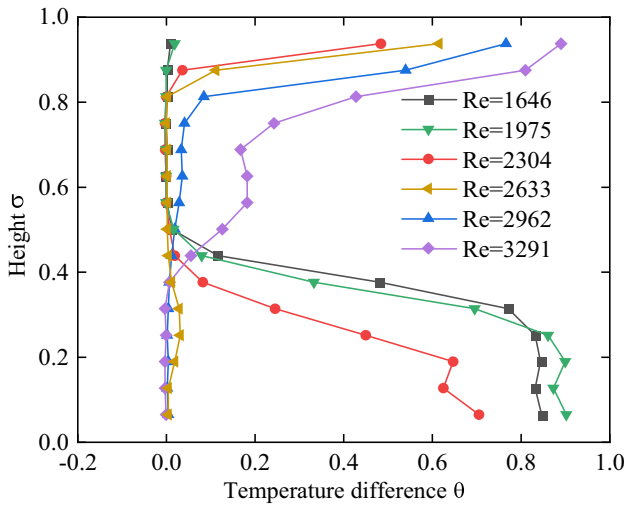

Fig. 9 The temperature change of L1 when Fo is 0.9

Figure 8 illustrates the variation of average outlet water temperature θ_o and Nu with different Re numbers in forward flow mode. It can be found that θ_o and Nu first decrease and then increase with flow rate. And θ_o and Nu have the minimum value at the Re of 2304.

As can be seen in Fig. 9, when Re is less than 2304, the closer the temperature measurement points are to the bottom of the sandbox, the greater the temperature change θ, while the temperature near the top of the sandbox remains almost constant; when Re is greater than 2633, the temperature change of L1 is the opposite, only the temperature on the top part of L1 changing. Besides, when Re is 2304, the temperature near both the top and bottom of the sandbox changes significantly, while it near the middle of the sandbox remains nearly unchanged. When Re is 2633, the temperature near the top of the sandbox changes significantly, while near the bottom changes slightly.

The change of temperature at the temperature measurement point means that heat exchange occurs at that location. The above phenomenon of temperature change

indicates that when Re is less than 2304, the heat exchange mainly occurs near the bottom of the sandbox; when Re is greater than 2633, the heat exchange mainly occurs near the top of the sandbox. In addition, when Re is 2304 and 2633, heat transfer occurs near both the top and bottom positions of the sandbox, but when Re is 2633, the convection heat transfer intensity at the bottom area is extremely low. Huang et al. (2018) studied a close-loop singe well geothermal heat exchanger similar to OBHE, and their results showed that the natural convection phenomenon in the reservoir is of great significance. Therefore, the effect of buoyancy should be taken into consideration when analyzing the reasons for the above phenomenon.

In the forward flow mode, without considering the effect of buoyancy, due to the influence of flow resistance, the pressure head at the inlet of the screen tube should be greater than that at the outlet of the screen tube. Thus, the possible flow tendency of water is to flow into the sandbox from the top area of the screen tube under the influence of the driving pressure difference and then flow back into the annuls from the bottom area of the sandbox. Moreover, as the inlet flow rate increases, the driving pressure difference between the inlet and outlet of the screen tube becomes greater, and the above trend becomes more obvious. Considering the influence of buoyancy force, as the convection heat transfer continues, the water temperature outside the screen tube gradually decreases, and the density of the water increases accordingly. Under the influence of the buoyancy force, the cold water tends to converge to the bottom of the sandbox. In summary, the fluid flow inside the sandbox is simultaneously affected by the driving effect of the fluid flow inside the screen tube and the buoyancy effect.

The above analysis can explain the change in the temperature field caused by the change in Re in Figs. 7 and 9. In the forward flow mode, the driving effect of the fluid flow inside the screen tube is opposite to the effect of buoyancy on the fluid flow inside the sandbox. When Re, which reflects the magnitude of the inlet flow rate under current conditions, is small, due to the small driving pressure difference, the effect of buoyancy is relatively greater, and the water flow shows a tendency to flow into the sandbox at the bottom area of the screen tube. On the contrary, when Re is large, the effect of buoyancy force becomes relatively small, and the water flow shows a tendency to flow into the sandbox from the top of the screen tube.

According to Fig. 9, when Re is larger than 2304, with the increase of the inlet flow rate, the temperature change of the temperature measurement point at the top area becomes larger. This can be explained that under the current flow conditions, the driving effect of the fluid in the screen tube plays a leading role in the fluid flow inside the sandbox, and thus as the increase in the flow rate, the driving pressure difference becomes larger, and the fluid is more likely to flow into the sandbox from the top area of the screen. When Re is smaller than 2304, only the temperature at the bottom part of L1 has changed, which means that the buoyance effect plays a dominant role in the formation of the convection heat transfer. Under this condition, a smaller inlet flow rate is supposed to be beneficial to the fluid flow into the sandbox from the bottom part of the screen tube. However, compared with Re of 2304, the temperature change of the bottom four temperature measurement points on L1 with Re of 1646 is relatively small. This may be because when Re is 1646, the heat exchange of the device is insufficient to reduce the temperature in the bottom area of sandbox to a lower level. But the fluid is indeed easier to flow into the

sandbox from the lower part of the screen, so the temperature changes at the 7th and 8th temperature measuring points from the bottom are greater when Re is 1646.

It can be concluded through further analysis that there must be an inlet flow rate, which can make the above two effects to a relatively balanced state. In this state, it is difficult for water to flow into the sandbox from neither the top part nor the bottom part of the screen tube. At this time, the convective heat transfer intensity is the lowest. The experimental conditions with Re of 2304 and 2633 are closer to this state. According to Figs. 8 and 9, in the above two flow rate conditions, the fluid flow into the sandbox from both the top and bottom area of the screen tube, but the temperature changes at the temperature measuring points are relatively small, and the heat transfer rate is lower than that of the other flow rate conditions, which is consistent with the previous deduction. The above analysis shows the correctness and accuracy of the previous analysis on the driving effect of fluid flow inside the screen tube and the buoyancy effect.

Influence of different fluid flow directions

According to the previous analysis, for the convective heat transfer effect inside and outside the screen tube in forward flow mode, the driving effect of fluid flow inside the screen tube and the buoyancy effect have opposite effects on the fluid flow trend inside the sandbox. Using the same analysis method, it can be concluded that the above two effects in backward flow mode have the same direction. It is thus speculated that the convective heat transfer effect will be enhanced and the water in the annulus will flow into the sandbox from the bottom area of the screen tube when the backward flow mode is adopted.

Therefore, experiments in backward flow mode are carried out to verify the above speculation. The inlet flow rates are, respectively, 0.3, 0.35, and 0.4 m^3/h, and the other conditions are the same as those in "Analysis of convection heat transfer characteristics in the sandbox" section, and the corresponding Reynolds numbers Re are 1975, 2304 and 2633, respectively. Figure 10 shows the variation of outlet temperature

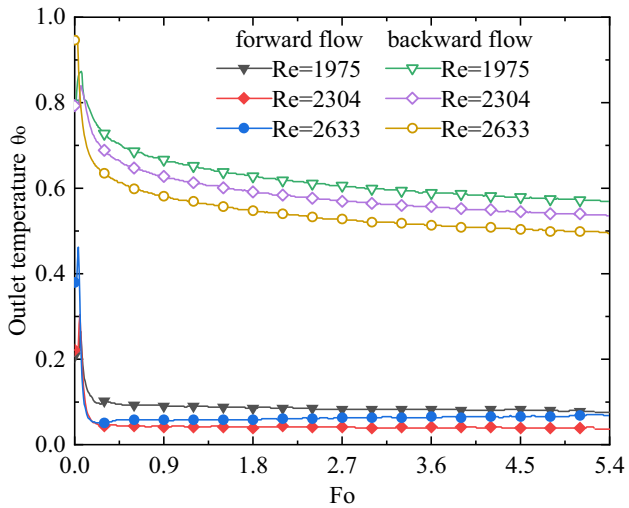

Fig. 10 The variation of outlet temperature with time in both flow modes

with time in both flow modes. As can be seen in the figure, the outlet temperature in backwards flow mode is obviously higher than that in forward flow mode, indicating that the convection heat transfer is enhanced in backward flow mode. This result is the same as the previous speculation. Besides, in backward flow mode, the outlet temperature decreases with the increase of Re, that is, the inlet flow rate, which is different from that in forward flow mode. Because the increase in heat transfer rate caused by the increasing flow rate is insufficient to heat the water temperature to a sufficiently high temperature. Moreover, it is speculated that the two driving effects mentioned above have the same direction, which means that the flow trend inside the sandbox will not change with the increase of inlet flow rate. That is, the outlet temperature and heat transfer rate in the backward flow mode will not change as in the forward flow mode shown in Fig. 8. However, the above speculation has not been fully proved, so it is necessary to further analyze the experiment results.

As shown in Fig. 11, under each Re condition, the temperature change at the middle and lower positions on L1 and L3 is large, and it is smaller as the temperature measurement points get closer to the top position, which shows that the heat transfer inside the sandbox in backward flow mode is mainly concentrated in the lower area. This is also consistent with the previous analysis. Figure 12 illustrates the temperature change of L2 in both flow modes when Fo is 1.8. Comparing the temperature changes of each temperature measurement point in the two flow modes, it can be seen that as the experiment continues, there are more temperature measurement points affected in backward flow conditions and the temperature change of the temperature point is also larger, which shows that the backward flow mode is more conducive to convection heat transfer inside and outside the screen tube. Besides, according to the above analysis, the fluid will flow into the sandbox from the bottom area of the screen tube in backward flow mode, which can be proved by Figs. 11 and 12. Therefore, the speculation that the two driving effects have the same direction in backward flow mode is correct.

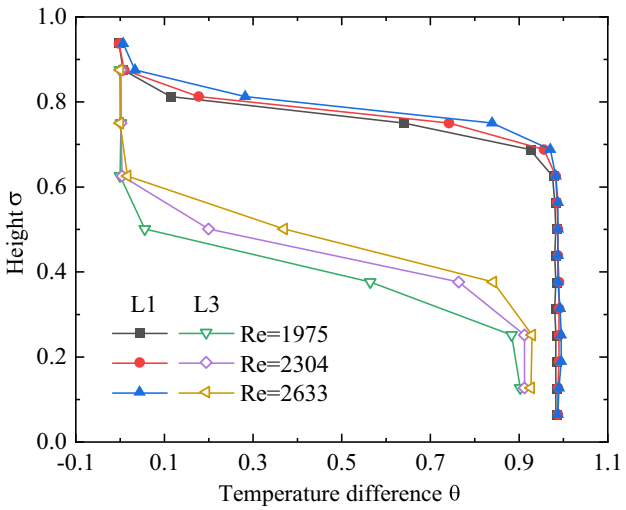

Fig. 11 Temperature changes of L1 and L3 in backward flow mode when Fo is 0.9

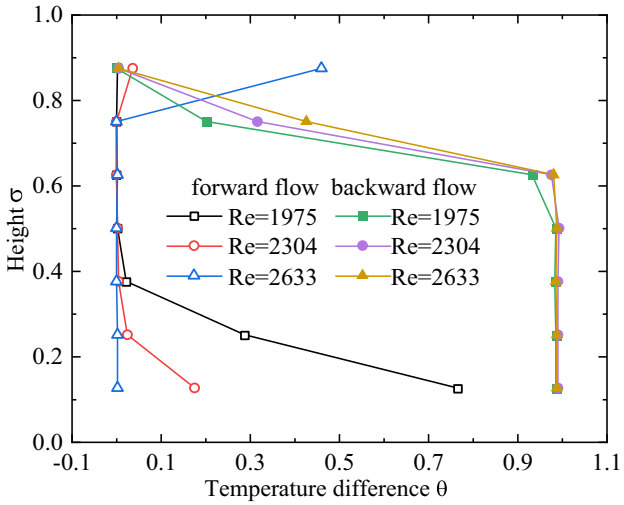

Fig. 12 Temperature change of L2 in both flow modes when Fo is 1.8

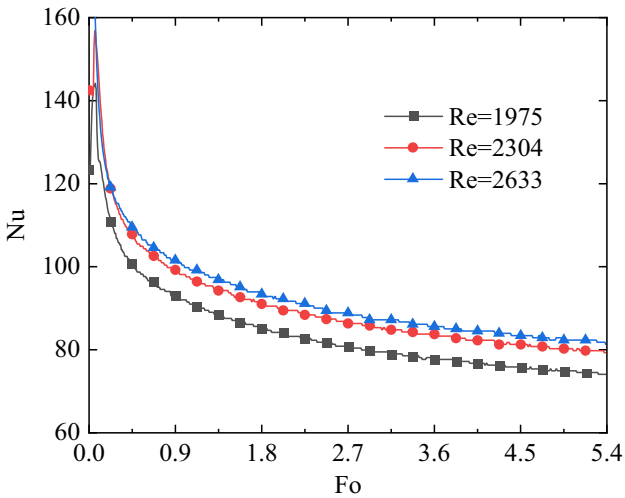

Fig. 13 Change of Nu with time in backward flow mode

In addition, it can be seen from Figs. 11 and 12 that in the backward flow mode, the temperature change of some measurement points near the top of the sandbox increases with the increase of Re, while it barely changes near the bottom of the sandbox due to the temperature being reduced to the same as the inlet temperature. Therefore, the convective heat transfer intensity inside and outside the screen increases with the increase of the Re, which can also be proved by Fig. 13. As shown in Fig. 13, the Nu of the experiment device increase with the increase of Re.

Effect of different inlet temperature

The convective heat transfer of OBHE in the reservoir area is affected by the buoyancy force, while the buoyancy force is driven by the fluid density difference caused by the fluid temperature difference, thus changing the inlet temperature will affect the fluid

flow field in the reservoir. In addition, the intensity of convective heat transfer is closely related to the heat transfer temperature difference, so the influence of the inlet temperature is analyzed in this section. The outer diameter of the inner tube is 20 mm, and the initial temperature of sandbox is 55 °C. The experiment results are listed in Table 1. The experimental results in Table 1 are not all in dimensionless form. Because this section only studies the influence of the inlet temperature on the heat transfer inside and outside the screen. It is intuitive and convenient to use the real outlet temperature and heat transfer rate for discussion. And the defined dimensionless outlet temperature in "Dimensionless parameters" section is not suitable for the discussion under current experimental conditions. In this section, the experiment in forward flow mode considers different inlet flow rates, while the experiment in backward flow mode only considers a single inlet flow rate. According to "Influence of different fluid flow directions" section, the driving effect of the fluid flow inside the screen tube and buoyancy effect act in the same direction in backward flow mode, thus the change of the inlet flow rate in this flow mode will not cause the change of the flow trend of the fluid inside the sandbox compared with that in the forward flow mode. Therefore, only a single inlet flow rate is used in the study of backward flow mode in this section and "Influence of different initial temperatures of reservoir" section.

It can be seen in Table 1 that under forward flow conditions, the average outlet temperature increases with the increase of the inlet temperature in both flow rate conditions. However, the variation of average heat exchange rate with inlet water temperature is different under the two flow rate conditions. As the inlet temperature rises, the average heat transfer rate decreases at Re of 1975, while it first decreases, then increases, and finally slightly decreases when Re is 2633. Besides, under the conditions with Re of 2633, there is a difference between the changing trend of heat exchange rate and Nu. Under backward flow mode conditions, the outlet temperature

Table 1 Experimental results for different inlet temperatures

Inlet temperature (°C)	Re	Flow mode	Sandbox temperature (°C)	Outlet temperature (°C)	Heat exchange rate (W)	Nu
10	1975	Forward	55	14.4	1547.7	9.7
14	1975	Forward	55	17.4	1176.1	8.0
16	1975	Forward	55	19.1	1074.1	7.7
18	1975	Forward	55	20.5	868.2	6.5
20	1975	Forward	55	22.2	765.4	6.0
10	2633	Forward	55	12.8	1300.1	8.0
14	2633	Forward	55	16.5	1144.9	7.7
16	2633	Forward	55	19.2	1462.3	10.5
18	2633	Forward	55	21.3	1515.1	11.5
20	2633	Forward	55	23.2	1488.4	11.9
12	1975	Backward	55	37.3	8817.0	77.7
14	1975	Backward	55	39.1	8738.5	82.1
16	1975	Backward	55	39.5	8158.2	80.0
18	1975	Backward	55	40.0	7658.5	78.8
20	1975	Backward	55	40.2	7020.0	75.4

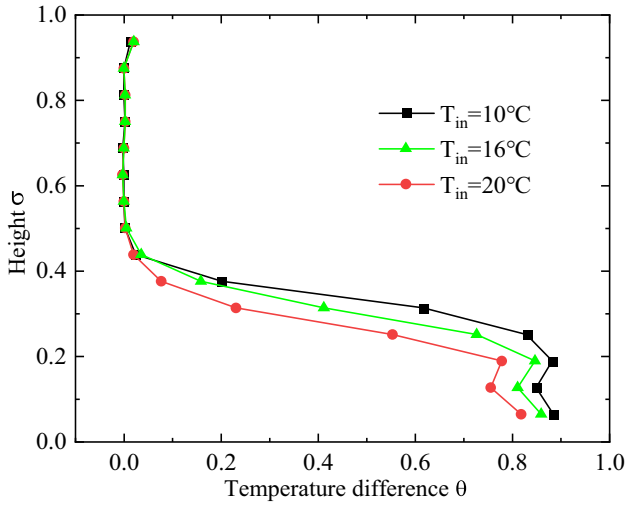

Fig. 14 Temperature change of L1 at different inlet temperatures when Re is 1975 and Fo is 0.9 in forward mode

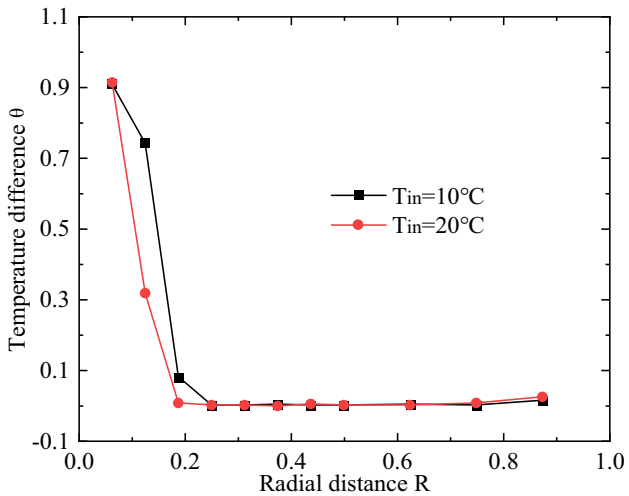

Fig. 15 Temperature change of L4 at different inlet temperatures when Re is 1975 and Fo is 0.9 in forward flow

rises slightly with the increase of inlet temperature, while the heat exchange rate decreases. Next, the above phenomenon will be analyzed in detail.

According to Fig. 9, under the condition that Re is 1975 and the inlet temperature is 14 °C, the fluid flows into the sandbox from the bottom area of the screen, that is, the buoyancy effect dominates the convection heat transfer process. With the increase of inlet temperature, the buoyancy effect driven by the temperature difference begins to decrease, which is not conducive for the fluid to flow into the sandbox. At the same time, the reduction of temperature difference is not conducive to heat transfer, so the heat exchange rate begins to decrease with the increase of inlet temperature. The above analysis can be proved by Figs. 14 and 15. Figure 14 shows that at different inlet temperature conditions, the heat exchange fluid flows into the sandbox from the

bottom area of the screen, and the smaller the inlet water temperature is, the greater the temperature difference, especially for the temperature measuring points near the bottom of the sandbox. Because under the current experimental conditions, as mentioned above, lower inlet water temperature is conducive to heat transfer. Figure 15 shows the temperature change of L4 when Re is 1975 and Fo is 0.9. It can be found that when the inlet temperature is 10 °C, the affected temperature field range is larger than that at the inlet temperature of 20 °C during the same operating time. When the inlet temperature is 10 °C, the temperature of the first three temperature measurement points closest to the screen tube on L4 changes, and when the inlet temperature is 20 °C, only the temperature of the first two temperature measurement points closest to the screen changes.

When Re is 2633, the variation of the heat transfer rate is relatively more complicated, but it is essentially the result of the combined action of driving effect of fluid flow inside the screen tube and buoyancy effect. Figure 16 illustrates the temperature change of L1 when Re is 2633 and Fo is 0.9. As shown in the figure, the temperature at both the top and bottom parts of L1 changes when the inlet temperature is 10 and 14 °C, which means that water flows into the sandbox from both the top and bottom area of the screen tube at the same time. However, the temperature change at the bottom part of L1 is not obvious, indicating that the convection heat transfer is much less intense at the bottom area, which has been analyzed in "Analysis of convection heat transfer characteristics in the sandbox" section. When the inlet temperature is 18 °C, only the temperature at the top part of the L1 changes, showing that the fluid flows into the sandbox only from the top area of the screen tube.

The above phenomenon shows that in addition to the inlet flow rate, the change of inlet temperature will also cause changes in the fluid flow field inside and outside the well. When the inlet temperature is 10 °C and 14 °C in forward mode, the fluid flows into the sandbox from the upper and lower sides of the screen tube at the same time. At this time, the convective heat transfer in the sandbox is in the process of transition

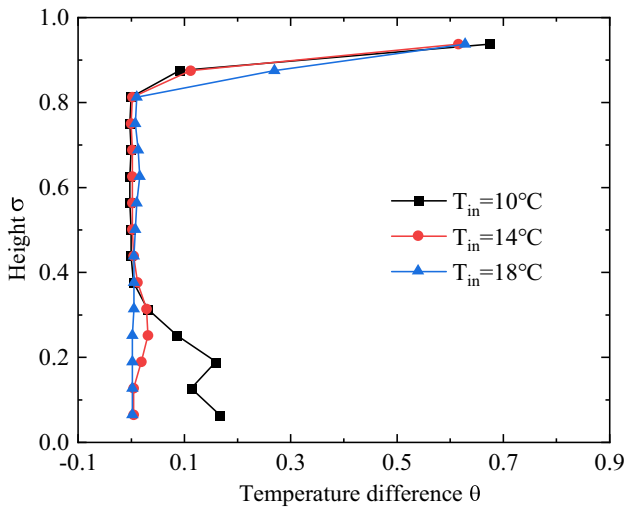

Fig. 16 Temperature change of L1 when Re is 2633 and Fo is 0.9 in forward mode

from being dominated by the buoyancy effect to being dominated by the driving effect of fluid flow inside the screen tube. In this process, the strength of the buoyancy effect is different according to the temperature difference between the inside and outside of the screen tube; thus the smaller the difference between the above two effects, the lower the driving force of fluid flow in the sandbox. This is the case when the inlet temperature is 14 °C, the heat transfer rate is low. When the inlet temperature is greater than 14 °C, the buoyancy effect is further reduced. Therefore, the driving effect of the fluid flow inside the screen becomes relatively greater, and the driving force of the fluid in the sandbox becomes greater, the above transition process is ended. At this time, the convective heat exchange effect begins to become stronger, and the heat transfer rate begins to increase. But when the inlet temperature is further increased, the temperature difference between the inside and outside of the screen tube becomes too small, causing the heat exchange rate to begin to decrease again. However, according to Nu, when the inlet temperature is 20 °C, the heat transfer coefficient still increases, but the increase degree begins to decrease. This proves that when the inlet temperature is 20 °C, the decrease of heat transfer rate is caused by the decrease of temperature difference inside and outside the screen tube.

According to "Influence of different fluid flow directions" section, the driving effect of fluid flow inside the screen tube and buoyancy effect acts in the same direction in backward flow mode. When the inlet temperature increases, the buoyancy effect begins to decrease due to the decrease of the fluid temperature difference, the driving force of the fluid flow inside the sandbox decreases, and the intensity of convective heat transfer inside and outside the screen tube decreases accordingly. Besides, the reduction of the temperature difference between the inside and outside of the screen tube is not conducive to heat exchange. Therefore, the heat transfer rate decreases with the increase of inlet temperature in backward flow mode. Although the decrease of heat transfer rate leads to the decrease of inlet and outlet temperature difference, the increasing extent of inlet temperature is greater, leading to the increase of outlet temperature.

Based on the above discussion, it can be found that raising the heat transfer temperature difference between the inside and outside of the screen tube may not necessarily improve the convection heat transfer rate in the reservoir area of OBHE in forward flow mode. When the convection heat transfer process is dominated by the buoyancy effect, reducing the inlet temperature can elevate the convection heat transfer rate; on the contrary, when the convection heat transfer process is dominated by the diving effect of fluid inside the screen tube, increasing the inlet temperature to a certain extent can increase the convection heat transfer intensity, but when the inlet temperature is too high, it will also cause a decrease in convection heat exchange rate of the reservoir area. When the backward flow mode is adopted, reducing the inlet temperature can enhance the convection heat transfer in the reservoir area.

Influence of different initial temperatures of reservoir

Since the change of the reservoir temperature can cause the temperature difference between the heat transfer fluid inside and outside the screen tube to change, this section will analyze the effect of different initial reservoir temperatures on the convective heat transfer inside and outside the screen tube. The inlet temperature is 14 °C, the outer

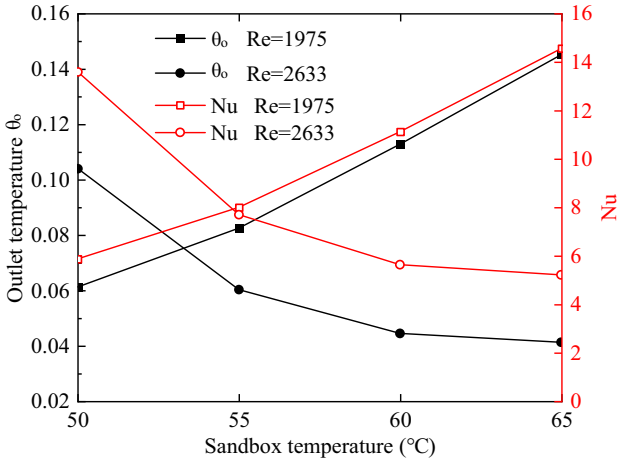

Fig. 17 The variation of average outlet temperature and Nu with the initial temperature of sandbox in forward flow mode

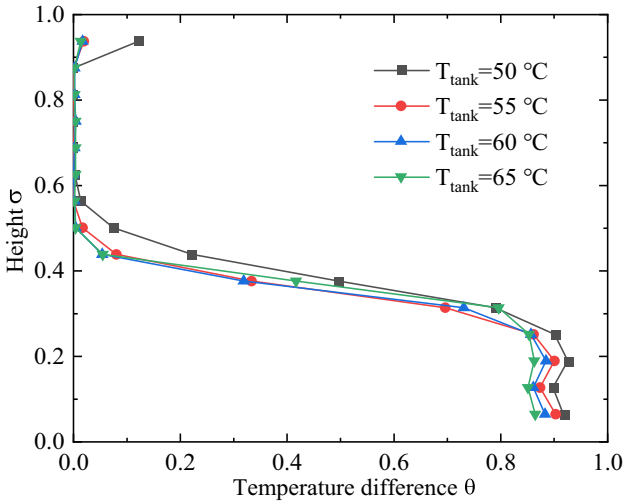

Fig. 18 Temperature changes of L1 when Re is 1975 and Fo is 0.9 in forward flow mode

diameter of the inner tube is 20 mm, the Re number in the forward flow mode is, respectively, 1975 and 2633, and it is 2633 in the backward flow mode.

Figure 17 illustrates the variation of average outlet temperature θ_o and Nu with the initial temperature of sandbox in forward flow mode. As can be seen in the figure, with the increase of the sandbox temperature, the variation of Nu has two completely different trends under two different inlet flow rates. θ_o and Nu increase with the increase of the initial sandbox temperature at Re of 1975, and decrease as the initial sandbox temperature rises at Re of 2633. However, the decreasing trend of θ_o and Nu when Re is 2633 gradually slows down with the increase of the sandbox temperature, and the downward trend stops finally.

Figure 18 shows the temperature change of L1 when Re is 1975 and Fo is 0.9 in forward flow mode. Under different initial sandbox temperature conditions, only the temperature of the lower part on L1 changes. Only when the temperature of the sandbox is

reduced to 50 °C, the uppermost on L1 has a relatively obvious temperature change. This means that under current conditions the fluid flows into the sandbox mainly from the bottom area of the screen tube, that is, the convection heat transfer process is dominated by the buoyancy effect. At this time, as the temperature of the sandbox increases, the temperature difference between the fluid in the screen tube and the fluid in the sandbox increases, resulting in the increase of buoyancy effect, which is beneficial for the fluid flow into the sandbox. In addition, the increasing temperature difference is also conducive to the progress of heat transfer. Therefore, the outlet temperature and heat exchange rate increase with the increase of the sandbox temperature. This is similar to the analysis of the influence of inlet temperature in "Effect of different inlet temperature" section, which is essentially a comprehensive change of convection and heat transfer caused by the increase in the temperature difference between the inside and outside of the screen tube.

Figure 19 illustrates the temperature change of L1 when Re is 2633 and Fo is 0.9 in forward flow mode. When the temperature of the sandbox is 50 °C, only the temperature of the upper part on L1 changes. This means that the fluid flows into the sandbox from the top area of the screen tube with Re of 2633 and sandbox temperature of 50 °C. As the temperature of the sandbox increases, the temperature of the lower part on L1 also begins to change. The higher the temperature of the sandbox is, the more temperature measuring points are affected, and the larger the temperature difference at those points near the bottom of the sandbox. It indicates that the fluid starts to flow into the sandbox from the bottom area of the screen tube when the temperature of the sandbox is greater than 50 °C, and the higher the sandbox temperature is, the more obvious this phenomenon is. When the temperature of the sandbox is 50 °C, the temperature difference between the inside and outside of the screen tube is small, resulting in a limited buoyancy effect. At this time, the driving effect of the fluid flow inside the screen tube dominates the convection heat transfer process. With the increase of the sandbox temperature, the buoyancy effect continues to rise, and the convective heat transfer in the sandbox begins to transform from being dominated by the driving effect of fluid

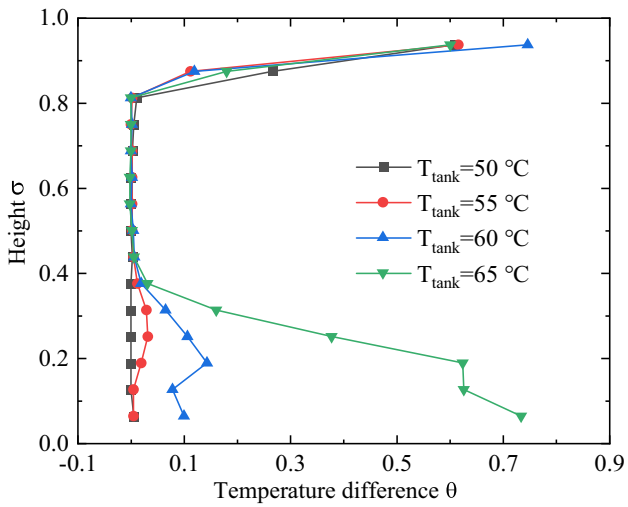

Fig. 19 Temperature changes of L1 when Re is 2633 and Fo is 0.9 in forward flow mode

flow inside the screen tube to being dominated by the buoyancy effect. During this process, the convection heat transfer intensity gradually decreases. It can be foreseen that as the temperature of the sandbox further increases, the buoyancy effect will be completely dominant in the convective heat transfer process, and the heat exchange rate will increase again.

According to the analysis in "Influence of different fluid flow directions" section, the driving effect of fluid flow inside the screen tube and the buoyancy effect act in the same direction in backward flow mode, thus, the enhancement of the buoyancy effect caused by the increase in the temperature difference between the inside and outside of the screen tube will improve the convection heat transfer inside and outside the screen tube. As shown in Fig. 20, the outlet temperature θ_o and Nu increase with the increase of the sandbox temperature, which proves the above analysis.

Effect of different inner tube sizes

As mentioned above, the factors that affect the convective heat transfer between the inside and outside of the screen tube include the driving effect of the fluid flow inside the screen tube and the buoyancy effect. The change in the size of the inner tube affects the driving pressure difference of the fluid flow in the screen tube, and thus influencing the convection heat transfer process. This section analyzes the influence of the outer diameter of the inner tube on the convective heat transfer between the inside and outside of the screen tube. The outer diameters of the inner tube are, respectively, 17, 20 and 23 mm, the inlet temperature is 18 °C and the initial sandbox temperature is 55 °C. The experimental conditions and experimental results are summarized in Table 2.

As shown in Table 2, the change of the inner tube diameter will change the outlet temperature. In forward flow mode, the outlet temperature decrease with increasing flow rate when the outer diameter of the inner tube is 17 mm, whereas they increase with increasing flow rate when the outer diameter is 20 or 23 mm. In addition, under the same inlet conditions, the change tendency of the outlet temperature with the pipe sizes varies according to the different inlet flow rates. As the diameter of the inner tube increases, the outlet temperature first decreases and then increases when the inlet flow

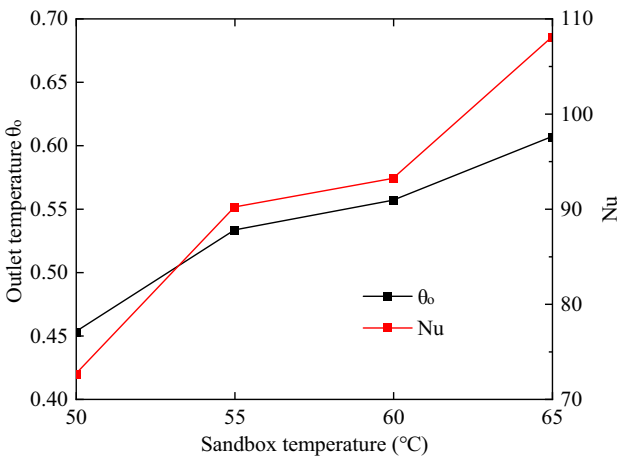

Fig. 20 Variation of average outlet temperature and Nu with sandbox temperature in backward flow mode

Table 2 Summary of the experimental conditions and results

Diameter (mm)	Flow mode	Flow rate (m^3/h)	Re	Outlet temperature θ_o
17	Forward	0.3	2092	0.13
17	Forward	0.4	2789	0.05
17	Forward	0.45	3138	0.02
20	Forward	0.3	1975	0.07
20	Forward	0.4	2633	0.09
20	Forward	0.45	2962	0.13
23	Forward	0.3	1870	0.13
23	Forward	0.4	2493	0.24
23	Forward	0.45	2805	0.28
17	Backward	0.4	2789	0.52
20	Backward	0.4	2633	0.53
23	Backward	0.4	2493	0.59

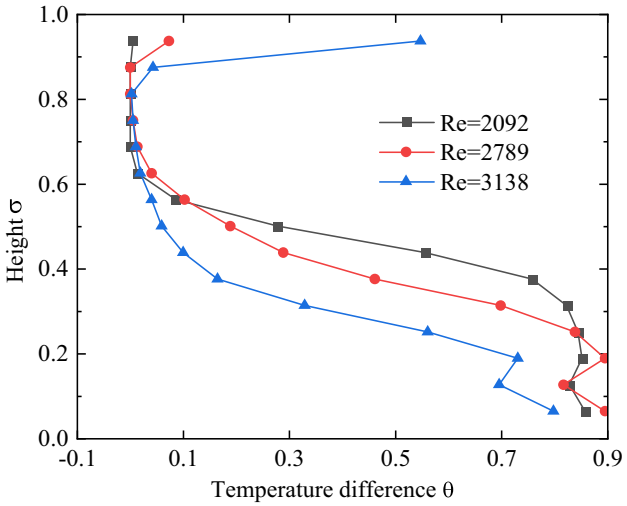

Fig. 21 Temperature change of L1 when Fo is 0.9 with inner tube diameter of 17 mm

rate is 0.3 m^3/h, while it continues to increase when the inlet flow rate is, respectively, 0.4 and 0.45 m^3/h. In backward flow mode, the outlet temperature gradually increase with the increase of inner tube diameter. Besides, when the inlet flow rate is constant, the change of Re is only caused by the change of inner pipe diameter. In this case, there is no obvious linear or other kinds of the corresponding relationship between the change of heat transfer rate and the change of Re numbers. This shows the complexity of the heat exchange mechanism in the reservoir area of OBHE, and the use of Re numbers alone cannot explain its heat exchange law very well.

Figure 21 shows the temperature change on L1 when Fo is 0.9 with an inner tube diameter of 17 mm. When Re is 2092, only the temperature on the bottom part of L1 changes, while it also changes on the top part of L1 when Re is, respectively, 2789 and 3138, and the temperature change on the top part of L1 is more obvious when Re is

3138. This means that, under the current conditions, when Re increases from 2092 to 3138, the convective heat transfer in the sandbox begins to transform from being dominated by the buoyancy effect to being dominated by the driving effect of fluid flow inside the screen tube. This process will cause the convection heat transfer rate to decrease, and the similar process has been analyzed many times before. However, comparing with Fig. 16, it can be found that for the inner tube with an outer diameter of 20 mm, this kind of transformation has been completed when Re is 2633, that is, the inlet flow rate is 0.4 m^3/h, at the same inlet temperature and sandbox temperature; at this time, the fluid flows into the sandbox from only the top of the screen tube, which shows that the diameter of the inner tube has a large influence on the exchange of fluids inside and outside the screen tube. It can be found in Fig. 22 that the above phenomenon is more obvious when the outer diameter of the inner tube is 23 mm. As can be seen in the figure, only the temperature of the top part on L1 changes under different Re conditions. That is because the fluid flows into the sandbox from only the top area of the screen under the current conditions.

The reason for the above phenomenon is that as the outer diameter of the inner tube increases, under the same flow condition, the flow rate of the fluid increases, and the driving pressure difference inside the screen tube increases. In forward flow mode, the driving effect of fluid flow inside the screen tube and the buoyancy effect act in different directions. Therefore, when the fluid flow inside the sandbox is dominated by the buoyancy effect, the increase in the inner tube diameter handers the convection heat transfer, which will lead to the decrease of the heat exchanger power between the inside and outside of the screen tube. On the contrary, when the fluid flow inside the sandbox is dominated by the driving effect of fluid flow inside the screen tube, the increase in the inner tube diameter will lead to the increase of the heat exchanger power. In backward flow mode, the above two effects act in the same direction, with the increase in the inner tube diameter, the increasing driving pressure difference will thus cause the increase in the convection heat exchanger power.

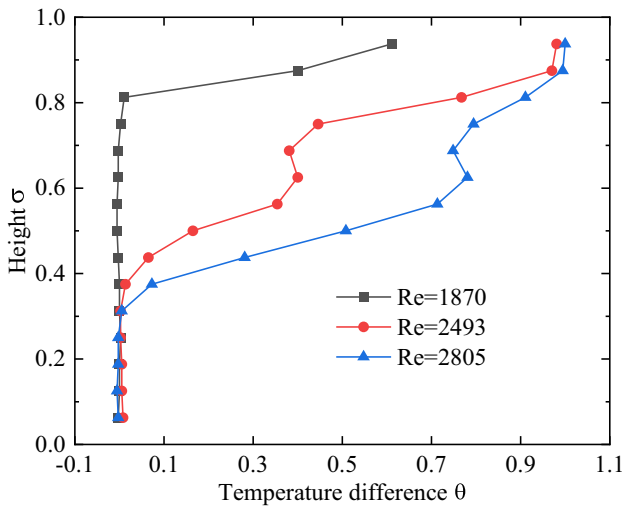

Fig. 22 Temperature change of L1 when Fo is 0.9 with inner tube diameter of 23 mm

Conclusions

DBHE technology relies on thermal conductivity to extract heat from low-conductivity rocks, and the heat exchange rate of a single well is thus limited. In contrast, OBHE utilizes an open-loop structure in the reservoir area that can realize convective heat transfer, and therefore its heat transfer rate is higher than that of DBHE (Dai et al. 2019a, b). OBHE is especially suitable for areas where the exploitation of groundwater is forbidden and where it is difficult to recharge. In this paper, a sandbox experiment platform is established to conduct a preliminary analysis of the convection heat transfer of OBHE in the reservoir. Besides, the influence of key factors on the convection heat transfer between the inside and outside of the screen tube is also studied. The main conclusions are as follows:

(1) Convection heat transfer between the inside and outside of the screen tube is simultaneously influenced by the driving effect of the fluid flow within the screen tube and the buoyancy effect. In forward flow mode, the aforementioned two effects operate in opposite directions, whereas in backward flow mode, they operate in the same direction. Therefore, the backward flow mode is more conducive to the extraction of heat from the OBHE reservoir area.
(2) Under the condition that both the inner tube and screen tube maintain the same diameter. In forward flow mode, the convection heat exchanger power decreases as the inlet flow rate increases when the buoyancy effect dominates the fluid flow inside the sandbox; on the contrary, it increases as the inlet flow rate increases. When the two driving effects have similar intensities, the convection heat exchange rate is relatively low. In backward flow mode, the convection heat exchange rate rises as the inlet flow rate rises.
(3) In forward flow mode, when the buoyancy effect is dominant, the convection heat exchanger power increases with the increase of temperature difference between the inlet flow and the sandbox; otherwise, it decreases with the increase of temperature difference. In backward flow mode, the convection heat exchange rate increases as the temperature difference increases.
(4) In forward flow mode, the convection heat exchanger power decreases with the increase of the inner tube size when the buoyancy effect is dominant; otherwise, it increases with the increase of the inner tube size, which is the same as the situation where the backward flow mode is adopted.
(5) In forward flow mode, when the buoyancy effect is dominant, the convection heat exchanger power decreases with the increase of the inner tube size; otherwise, it increases with the increase of the inner tube size, which is the same as when the backward flow mode is used.

The sandbox experiment designed in this paper does not consider the similarity criteria, it is also impossible to predict the convective heat transfer rate of OBHE in the reservoir area through experiments. However, the sandbox experiment results are useful for analyzing the convective heat transfer mechanism in the reservoir region and establishing a foundation for future studies of OBHE.

Acknowledgements
This work was supported by the "Transformational Technologies for Clean Energy and Demonstration", Strategic Priority Research Program of the Chinese Academy of Sciences, Grant No. XDA 21000000, and by the National Natural Science Foundation of China (No. 41972314)

Author contributions
KJ: experiment, formal analysis, writing—original draft. XB: conceptualization, methodology, writing—review and editing, funding acquisition. HL: methodology. FM: conceptualization. LW: formal analysis, writing—original draft. All authors read and approved the final manuscript.

Funding
This study was supported by National Natural Science Foundation of China (Grant No. 41972314).

Availability of data and materials
The datasets used and/or analyzed during this investigation are accessible upon reasonable request from the corresponding author.

Declarations

Competing interests
The authors declare that they have no competing interests.

Received: 9 December 2022 Accepted: 11 April 2023
Published online: 20 April 2023

References

Barbier E. Geothermal energy technology and current status: an overview. Renew Sustain Energy Rev. 2002;6:3–65.
Beier RA, Smith MD, Spitler JD. Reference data sets for vertical borehole ground heat exchanger models and thermal response test analysis. Geothermics. 2011;40:79–85.
Bu XB, Ma WB, Li HS. Geothermal energy production utilizing abandoned oil and gas wells. Renew Energy. 2012;41:80–5.
Bu X, Ran Y, Zhang D. Experimental and simulation studies of geothermal single well for building heating. Renew Energy. 2019;143:1902–9.
Cai WL, Wang FH, Liu J, et al. Experimental and numerical investigation of heat transfer performance and sustainability of deep borehole heat exchangers coupled with ground source heat pump systems. Appl Thermal Eng. 2019;149:975–86.
Cheng WL, Li TT, Nian YL, et al. Studies on geothermal power generation using abandoned oil wells. Energy. 2013;59:248–54.
Cheng WL, Liu J, Nian YL, et al. Enhancing geothermal power generation from abandoned oil wells with thermal reservoirs. Energy. 2016;109:537–45.
Dai C, Li J, Shi Y, et al. An experiment on heat extraction from a deep geothermal well using a downhole coaxial open loop design. Appl Energy. 2019a;252: 113447.
Dai C, Shi Y, Zeng L, et al. Heat extraction performance of a deep downhole heat exchanger. Energy Procedia. 2019b;158:5602–7.
Davis AP, Michaelides EE. Geothermal power production from abandoned oil wells. Energy. 2009;34:866–72.
Deng Z, Rees SJ, Spitler JD. A model for annual simulation of standing column well ground heat exchangers. Hvac&r Res. 2005;11:637–55.
Deng JW, Wei QP, He S, et al. Simulation analysis on the heat performance of deep borehole heat exchangers in medium-depth geothermal heat pump systems. Energies. 2020;13:28.
Fang L, Diao N, Shao Z, et al. A computationally efficient numerical model for heat transfer simulation of deep borehole heat exchangers. Energy Build. 2018;167:79–88.
He YJ, Bu XB. A novel enhanced deep borehole heat exchanger for building heating. Appl Thermal Eng. 2020;178:6.
Holmberg H, Acuna J, Naess E, et al. Thermal evaluation of coaxial deep borehole heat exchangers. Renew Energy. 2016;97:65–76.
Hu XC, Banks J, Wu LP, et al. Numerical modeling of a coaxial borehole heat exchanger to exploit geothermal energy from abandoned petroleum wells in Hinton, Alberta. Renew Energy. 2020;148:1110–23.
Huang WB, Cao WJ, Jiang FM. A novel single-well geothermal system for hot dry rock geothermal energy exploitation. Energy. 2018;162:630–44.
Huang Y, Zhang Y, Xie Y, et al. Field test and numerical investigation on deep coaxial borehole heat exchanger based on distributed optical fiber temperature sensor. Energy. 2020;210: 118643.
Huang Y, Zhang Y, Xie Y, et al. Long-term thermal performance analysis of deep coaxial borehole heat exchanger based on field test. J Clean Prod. 2021;278: 123396.
Jiang K, Bu X. Simulation analysis of a single well geothermal system with open-loop structure. Geothermics. 2022;100: 102338.
Kalmar L, Medgyes T, Szanyi J. Specifying boundary conditions for economical closed loop deep geothermal heat production. Energy. 2020;196:21.
Kujawa T, Nowak W, Stachel AA. Utilization of existing deep geological wells for acquisitions of geothermal energy. Energy. 2006;31:650–64.

Liu ZJ, Xu W, Qian C, et al. Investigation on the feasibility and performance of ground source heat pump (GSHP) in three cities in cold climate zone, China. Renew Energy. 2015;84:89–96.
Liu J, Wang FH, Cai WL, et al. Numerical study on the effects of design parameters on the heat transfer performance of coaxial deep borehole heat exchanger. Int J Energy Res. 2019;43:6337–52.
Liu J, Wang F, Gao Y, et al. Influencing factors analysis and operation optimization for the long-term performance of medium-deep borehole heat exchanger coupled ground source heat pump system. Energy Build. 2020;226: 110385.
Lund A, Karvinen T, Lehtonen M. Analysis of deep-heat energy wells for heat pump systems. In: 2020 IEEE PES innovative smart grid technologies Europe (ISGT-Europe); 2020.
Luo YQ, Guo HS, Meggers F, et al. Deep coaxial borehole heat exchanger: analytical modeling and thermal analysis. Energy. 2019;185:1298–313.
Luo YQ, Yu JH, Yan T, et al. Improved analytical modeling and system performance evaluation of deep coaxial borehole heat exchanger with segmented finite cylinder-source method. Energy Build. 2020;212:16.
Ma L, Zhao YZ, Yin HM, et al. A coupled heat transfer model of medium-depth downhole coaxial heat exchanger based on the piecewise analytical solution. Energy Convers Manag. 2020;204:17.
Morchio S, Fossa M. Thermal modeling of deep borehole heat exchangers for geothermal applications in densely populated urban areas. Thermal Sci Eng Prog. 2019;13: 100363.
Morchio S, Fossa M, Priarone A, et al. Reduced scale experimental modelling of distributed thermal response tests for the estimation of the ground thermal conductivity. Energies. 2021;14:6955.
Morchio S, Fossa M, Beier RA. Study on the best heat transfer rate in thermal response test experiments with coaxial and U-pipe borehole heat exchangers. Appl Thermal Eng. 2022;200: 117621.
Morita K, Bollmeier WS, Mizogami H. Analysis of the results from the downhole coaxial heat exchanger (DCHE) experiment in Hawaii. Geothermal Resources Council; 1992a.
Morita K, Bollmeier WS, Mizogami H. An experiment to prove the concept of the downhole coaxial heat-exchanger (DCHE) in Hawaii. 20th anniversary-Geothermal Resources Council. Geothermal Resources Council. 1992b;16:9–16.
Nian Y-L, Cheng W-L. Evaluation of geothermal heating from abandoned oil wells. Energy. 2018;142:592–607.
Noorollahi Y, Pourarshad M, Jalilinasrabady S, et al. Numerical simulation of power production from abandoned oil wells in Ahwaz oil field in southern Iran. Geothermics. 2015;55:16–23.
Pan AQ, Lu L, Cui P, et al. A new analytical heat transfer model for deep borehole heat exchangers with coaxial tubes. Int J Heat Mass Transf. 2019;141:1056–65.
Pan S, Kong YL, Chen CF, et al. Optimization of the utilization of deep borehole heat exchangers. Geotherm Energy. 2020;8:20.
Rees SJ, Spitler JD, Deng Z, et al. A study of geothermal heat pump and standing column well performance. ASHRAE Trans. 2004;110:3–13.
Shirazi AS, Bernier M. A small-scale experimental apparatus to study heat transfer in the vicinity of geothermal boreholes. Hvac&r Res. 2014;20:819–27.
Song W, Ni L, Yao Y. Experimental research on the characteristics of single-well groundwater heat pump systems. Energy Build. 2019;191:1–12.
Stefánsson V. World geothermal assessment. In: Proceedings of the world geothermal congress. Antalya, Turkey; 2005.
Suganthi L, Samuel AA. Energy models for demand forecasting—a review. Renew Sustain Energy Revi. 2012;16:1223–40.
Sutton MG, Nutter DW, Couvillion RJ. A ground resistance for vertical bore heat exchangers with groundwater flow. J Energy Res Technol. 2003;125:183–9.
Wang ZH, Wang FH, Liu J, et al. Field test and numerical investigation on the heat transfer characteristics and optimal design of the heat exchangers of a deep borehole ground source heat pump system. Energy Convers Manag. 2017;153:603–15.
Wang G, Song X, Shi Y, et al. Production performance of a novel open loop geothermal system in a horizontal well. Energy Convers Manag. 2020;206: 112478.
Xia LY, Zhang YB. An overview of world geothermal power generation and a case study on China—the resource and market perspective. Renew Sustain Energy Rev. 2019;112:411–23.
Zhao J, Wang H, Li X, et al. Experimental investigation and theoretical model of heat transfer of saturated soil around coaxial ground coupled heat exchanger. Appl Thermal Eng. 2008;28:116–25.

Publisher's Note